Edited by Martin H. G. Prechtl

Nanocatalysis in Ionic Liquids

WILEY-VCH
Verlag GmbH & Co. KGaA

Editor

Dr. Martin H. G. Prechtl
Universität zu Köln
Institut für Anorganische Chemie
Greinstr. 6
50939 Köln
Germany

Cover
A TEM image of nanoparticles was kindly provided by the editor.

Library of Congress Card No.: applied for

British Library Cataloguing-in-Publication Data
A catalogue record for this book is available from the British Library.

Bibliographic information published by the Deutsche Nationalbibliothek
The Deutsche Nationalbibliothek lists this publication in the Deutsche Nationalbibliografie; detailed bibliographic data are available on the Internet at <http://dnb.d-nb.de>.

Print ISBN: 978-3-527-33910-5
ePDF ISBN: 978-3-527-69412-9
ePub ISBN: 978-3-527-69413-6
Mobi ISBN: 978-3-527-69414-3
oBook ISBN: 978-3-527-69328-3

Cover Design Adam Design Weinheim, Germany
Typesetting SPi Global, Chennai, India
Printing and Binding

Printed on acid-free paper

13
Photovoltaic, Photocatalytic Application, and Water Splitting

Adriano F. Feil, Heberton Wender, and Renato V. Gonçalves

13.1
Introduction

Owing to population growth in recent decades, governments worldwide have faced numerous environmental problems and an energy shortage with an acceptable cost-benefit ratio [1]. Both energy generation and wastewater treatment must be based on sustainable, environmentally friendly, and low-cost processes. Furthermore, they must be carbon-free, and not discharge toxic or harmful by-products into the environment [2, 3]. Moreover, energy must be produced by abundant earth materials and renewable resources, focusing on the development of new technologies to replace oil derivatives, whose processing dumps millions of tons of toxins into the atmosphere [4]. A renewable resource such as solar energy has more than enough potential to supply the world's energy demands if part of its radiation could be absorbed through environmentally clean processes [5].

In this chapter we will highlight three different and important processes that use solar energy to convert photons into electricity and decontaminate wastewater in the presence of a nanocrystal semiconductor synthesized in ionic liquid (IL) media, namely, solar cells, photocatalytic wastewater treatment, and photo and photoelectrocatalytic water splitting (WS). Solar cells are regarded as a renewable alternative for converting energy from the sun into electricity through a clean and environmentally friendly process. The total cost per watt peak has decreased over the years at the same time as cells have become more efficient [6]. Also showing promise [7, 8], the direct photocatalytic splitting of water into hydrogen and oxygen has been the subject of thousands of papers over the past four decades. The hydrogen generated could provide a sustainable source for the generation of industrially important gases, vehicular fuel, and as a storage medium for solar energy [9–11]. In addition, industrial waste discharge of domestic sewage, and emerging contaminants such as pesticides, hormones, and drugs, among others, deserve special attention [12]. Sunlight has been employed to decontaminate water by using a semiconductor material capable of efficiently absorbing photons, generating electrons, and holes in their conduction

Nanocatalysis in Ionic Liquids, First Edition. Edited by Martin H.G. Prechtl.

and valence band (VB), respectively, with the potential to create chemically reactive species in water that can destroy organic pollutants. This process can be used in conjunction with conventional water treatments to eliminate resistive compounds.

13.2 Photovoltaic Cells

Solar energy is one of the main freely available renewable energy sources that can be harvested to meet future energy requirements. Dye-sensitized solar cells (DSSCs) are an economically viable alternative to conventional inorganic photovoltaic devices to convert solar energy into electricity [13–16]. DSSCs are easy to handle, prepare, and assemble in addition to exhibiting acceptable conversion efficiencies.

13.2.1 Working Principles of a DSSC

A DSSC is composed of different layers that play a key role in its operation. Figure 13.1 shows a schematic overview of a DSSC. Solar cells are always constructed on top of conducting glass as an anode electrode (or plastic substrates in the case of flexible devices). The most widely used is glass coated with fluorine-doped tin oxide (FTO) to support the solar cell layers. The support substrate must be transparent in the visible and near UV region because light is coupled into the cell through the substrate. The heart of the device on the surface of the FTO layer consists of nanocrystalline films composed of a mesoporous oxide layer, such as TiO_2 nanoparticles, to establish electronic conduction. Oxide film thickness is typically ~10 μm, and nanoparticle size 10–30 nm in diameter with porosities of ~50–60% [15]. This nanoparticle layer is impregnated with a charge transfer dye and placed in contact with a triiodide/iodide redox couple electrolyte. The outer layer is a counter electrode usually composed of a Pt film deposited on an FTO/glass.

The mechanism of photon-to-current conversion will be briefly explained. The organic dye absorbs photons from the sun, generating electron–hole pairs. The photoexcited electrons generated in the dye molecules are injected into the conduction band of the oxide, leaving the dye in an intermediate oxidized state. The dye is restored to its ground state by electron transfer from the electrolyte that undergoes oxidation from I^- to I_3^- at this stage. Since the oxide is an n-type semiconductor, the electrons flow through an external circuit to the FTO and return to the other counter electrode. At this stage, the electron is transferred to the electrolyte (or a hole-conducting material in the case of solid DSSCs) to regenerate it to I^-.

DSSCs were originally composed of liquid electrolytes to provide high power conversion efficiency. Unfortunately, these liquid electrolytes face complications

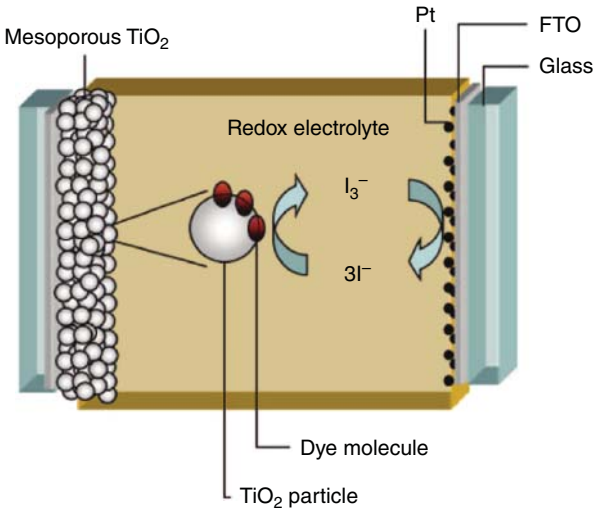

Figure 13.1 Schematic overview of a dye-sensitized solar cell [15]. (Hagfeldt *et al*. [15]. Reproduced with permission of American Chemical Society.)

in long-term practical use. Problems such as evaporation, leakage, desorption of loosely attached dye, photodegradation in the desorbed state, ineffective sealing of cells, and corrosion of the Pt counter electrode by the triiodide/iodide couple, are some of the critical factors limiting the long-term performance of DSSCs, especially at high temperatures [17, 18]. Thus, in order to overcome these drawbacks, solid and quasi-solid (gel-like) electrolytes using ILs have emerged as promising alternatives to replace liquid electrolytes. This is discussed in detail in the following subsections.

13.2.2
ILs in Photovoltaic Cells

Owing to specific properties such as low volatility, high electrochemical and thermal stability, and high ionic conductivity, ILs have been widely used as primary electrolytes [19–21], additives for increasing ionic conductivity in gel polymer-based electrolytes [22], and as cathode interfacial layers [23], all in regard to efficient conversion of solar energy to electrical current.

ILs were first used as an important source for iodide-based redox couples and as a solvent in DSSCs [24]. Since ILs are viscous media, a number of authors have studied the effect of viscosity on DSSC efficiency. Short-circuit photocurrent and conversion efficiency increases with a decrease in the viscosity of room temperature ILs, as in conventional electrolytes [19]. Conversion efficiency was very low (around 2%) at the beginning. Room-temperature molten salt systems based on 1-hexyl-3-methylimidazolium iodide ($[C_6mim][I]$) exhibited a number of advantages over organic liquids as solvents for solar cell electrolytes, such as

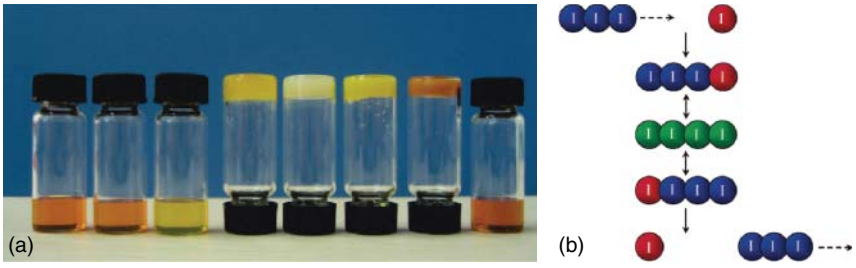

Figure 13.2 (a) Photographs of imidazolium melts and their mixtures at room temperature. The samples from left to right are $[C_6mim][I]$, $[C_4mim][I]$, $[C_3mim][I]$, $[C_2mim][I]$, $[C_1mim][I]$, $[C_1mim][I]/[C_2mim][I]$ (1/1, molar ratio), 1-allyl-3-methylimidazolium iodide ([Amim][I]), $[C_1mim][I]/[C_2mim][I]/[Amim][I]$ (1/1/1, molar ratio), respectively. All samples were dried at 80 °C under a vacuum of ~3 Torr for 8 h. (b) Schematic coupling transport mechanism of triiodide in IL electrolytes with a high iodide packing density, where the red, blue, and green balls represent the iodide, triiodide, and encountering complex, respectively [25]. (Cao *et al*. [25]. Reproduced with permission of American Chemical Society.)

outstanding stability [21]. Different types of ILs were combined with iodine to form a redox couple in DSSC devices [20]. The authors reported that the structure and property of the ILs had a significant influence on DSSC performance. Ionic conductivity (viscosity) and charge transport by the exchange reaction between the iodide/triiodide redox couple played an important role in efficiency, reaching 5.5% under optimized conditions.

By systematically revising the temperature-dependent physicochemical properties (density, conductivity, and fluidity) of 1,3-dialkylimidazolium iodides, Wang *et al.* [25] found that using low-viscosity iodide melts with small cations resulted in high-efficiency DSSCs. Figure 13.2a shows photographs of imidazolium melts and their mixtures at room temperature. Employing high-fluidity, eutectic-based melts considerably increased the efficiency of the device compared to those for cells with corresponding state-of-the-art IL electrolytes (from 3% to 7%). The authors proposed a modified Stokes-Einstein equation by correlating ion mobility and fluidity to quantitatively describe triiodide transport in IL electrolytes. Apart from normal physical diffusion, the coupling process of physical diffusion and bond exchange, as shown in Figure 13.2b, was used to explain the viscosity-dependent transport of triiodide in IL electrolytes with a high iodide concentration. It was concluded that triiodide approaches iodide from one end, forming an encounter complex, from which triiodide is released at the other end.

Quasi-solid-state DSSCs were fabricated by introducing low-molecular-weight "gelator" (Scheme 13.1) into the cell electrolyte [17]. In this study, viscosity and ionic conductivity also played special roles in the high photoconversion efficiency of the mechanism.

Several authors have investigated these ionic polymer-based quasi-solid-state DSSCs [18, 22]. Cells with IL polymer gel containing 1-methyl-3-propylimidazolium iodide ($[C_3mim][I]$) and photochemically stable poly

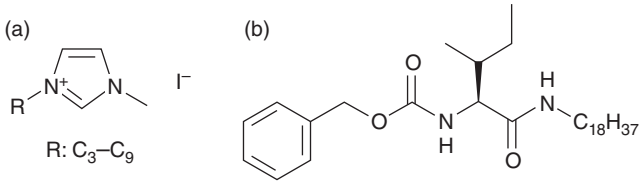

Scheme 13.1 Chemical structures of (a) 1-alkyl-3-methylimidazolium iodides and (b) gelator [17].

(vinylidenefluoride-co-hexafluoropropylene), combined with hydrophobic dye Z907-coated TiO_2 nanoparticles, showed an overall conversion efficiency of 5.3% at AM1.5 illumination. In this case, IL polymer gel electrolytes offered the same benefits as ILs, but with an all solid-state structure that presented new possibilities for preparing flexible devices.

A sol–gel electrolyte nanocomposite containing silica nanoparticles and a mixture of surfactants, including IL $[C_3mim][I]$ mixed iodine as I^{3-}/I^- redox couple in its organic subphase, resulted in an overall solar cell efficiency of 5.4%. Grätzel *et al.* [26] were the first to show that the gelation of ILs with SiO_2 nanoparticles was an efficient method for preparing quasi-solid-state DSSCs, with efficiencies around 7% at AM1.5 sunlight in combination with an amphiphilic ruthenium polypyridyl photosensitizer, very similar to results found using liquid electrolytes as control. Subsequent to this study, other groups also started introducing nanomaterial in ILs to obtain gel-like electrolytes. SiO_2 nanoparticles were also used to solidify polymers and then blended with ILs to prepare efficient gel-like electrolytes for DSSCs [27]. In this article, the quasi-solid electrolyte is modified using $[C_3mim][I]$ rather than solid 1,2-dimethyl-propylimidazolium iodide ($[C_3C_1mim][I]$) as iodide source to enhance the conversion efficiency (~7%).

Usui *et al.* [28] studied the effect of adding nanoparticles to a DSSC/IL electrolyte. Carbon nanotubes, other carbon nanoparticles, and titanium dioxide nanoparticles were dispersed individually into a 1-ethyl-3-methylimidazolium bis(trifluoromethylsulfonyl)imide ($[C_2mim][N(Tf)_2]$) IL electrolyte, resulting in ionic nanocomposite gel electrolytes. With the addition of nanoparticles, IL viscosity and electric conductivity increased substantially, leading to improvements in photovoltaic performance. Figure 13.3a shows the open-circuit voltage (V_{oc}), short-circuit current (J_{sc}), efficiency (η), and fill factor (FF) plot of devices prepared using different nanoparticles including multiwalled carbon nanotubes (MWCNTs), single-walled carbon nanotubes (SWCNTs), carbon fibers (CFs), and carbon black nanoparticles. The best efficiencies were found for TiO_2, followed by carbon black nanocomposite-based gel electrolytes. The chemical structure of IL used is presented in Figure 13.3b. The IL was strongly solidified after the addition of nanoparticles, Figure 13.3c. Agarose/TiO_2-containing IL electrolyte improved not only photovoltaic efficiency but also long-term performance stability of DSSC [30]. The improved cell efficiency was correlated to the longer electron lifetime, higher ion diffusivity, and the lower electrical resistance obtained in the electrolyte.

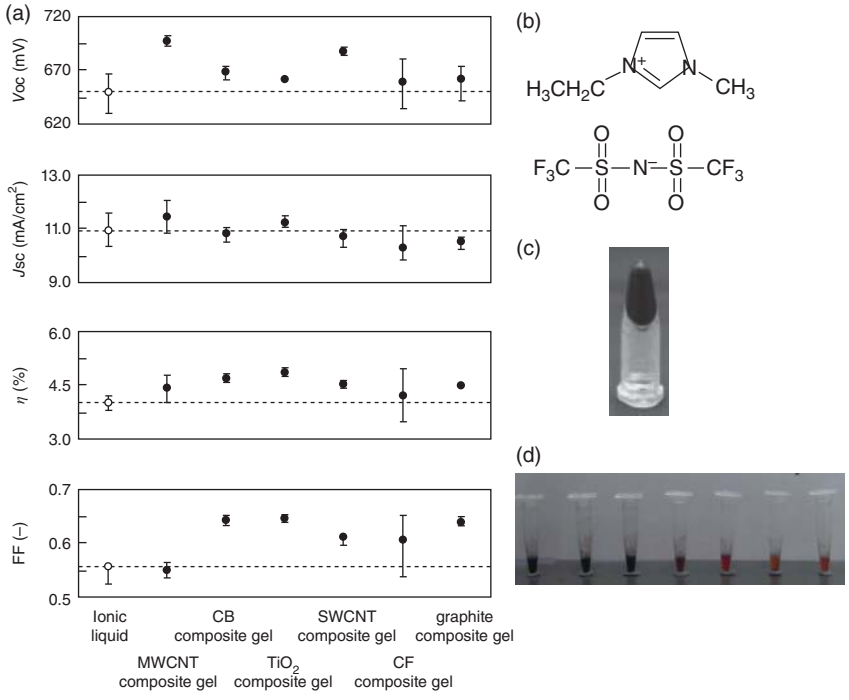

Figure 13.3 (a) Plots of V_{oc}, J_{sc}, η, FF versus ionic liquid electrolytes and ionic nanoparticle gel electrolytes. A white circle and a dashed line show the value of the DSCs with ionic liquid electrolytes alone ($n = 3$). (b) Scheme of $[C_2mim][N(Tf)_2]$ chemical structure. (c) Picture of the ionic nanocomposite gel containing MWCNTs. These were ground with $[C_2mim][N(Tf)_2]$ in an agate mortar and then centrifuged [28]. (d) Photographic images of graphene-ionic liquid electrolytes with graphene concentration increasing from right to left [29]. (Usui *et al*. [28]. Reproduced with the permission of Elsevier.)

More recently, graphene, SWCNTs, and a mixture of graphene and SWCNTs were incorporated into $[C_3mim][I]$ IL. An increase in light conversion efficiency was observed because carbon materials act simultaneously as both charge transporter in the ILs and catalyst for the electrochemical reduction of I^3. In addition, interactions between graphene and the IL system lead to the formation of self-organized assemblies or networks [29]. These factors not only provided an efficient electron transfer network through the electrolyte but also allowed for the formation of quasi-solid electrolytes at higher graphene concentrations (Figure 13.3d). Without any volatile organic solvent, DSSCs based on composite electrolytes containing GO showed higher power conversion efficiency and better long-term stability compared to those without GO [31].

More than 10% efficiency was recently reported for inverted polymer solar cells (i-PSCs) with a ZnO/IL combined cathode interfacial layer [23]. In the i-PSCs, interlayers between the active layer and ITO have been used to reduce the work

function of ITO and improve electron collection for photon-to-current efficiency (PCE) enhancement. Modification of ITO and ZnO with the IL layer increased the efficiency of the device (J_{sc}, FF, and PCE) due to the reduction in cathode work function by forming spontaneous dipolar polarization at the interface. ILs were also used as interfacial layer in hybrid quantum dot-organic solar cells (HyQD-OSCs). The insertion of an IL layer between PbS and phenyl-C61-butyric acid methyl ester (PCBM) could shift the band edge of PCBM closer to the vacuum level of PbS owing to spontaneous dipole polarization. As a result, improvements in performance were achieved, including increases in open-circuit voltage, fill factor, and power conversion efficiency [32].

13.3 Photocatalytic Processes

Heterogeneous photocatalysis is one of the most important reactions to environmental applications for removal of various types of organic/inorganic compounds in wastewater due to the increased industrial discharge of contaminants into clean water sources. A photocatalytic reaction is traditionally performed using transition metal oxides and titanium dioxide (TiO_2) has been established as the most promising photocatalyst material for degrading (mineralization) different pollutant compounds, such as phenols, organic dyes, carboxylic acid, drugs, herbicides, and insecticides [33–35].

13.3.1 Principles of Photocatalysis

A brief description of the principles of photocatalysis using semiconductor materials is presented here. A more detailed discussion can be found in [33]. The process of semiconductor photocatalysis involves the following steps [36, 37]:

- *Photoexcitation*: The photoexcitation process is based on photon absorption events (photons with energies higher than the bandgap of the semiconductor) that promote electrons from the VB to the empty conduction band (CB);
- *Charge separation event*: Formation of electron–hole pairs (e^-, h^+) and migration to surface reaction sites.

Figure 13.4 outlines the basic working principle of photocatalysis. At the outset, a photon with energy higher than the material bandgap is absorbed by an electron in VB, and is then promoted to the CB, leaving a hole in the VB. After this photoexcitation, the electron–hole pairs (e^-, h^+) formed in the structure of the photocatalyst material can migrate to its surface, inducing a series of reductive and oxidative reactions in the presence of adsorbed electron donors (or acceptors); or recombine in a defect, dissipating the input energy as heat [39, 40].

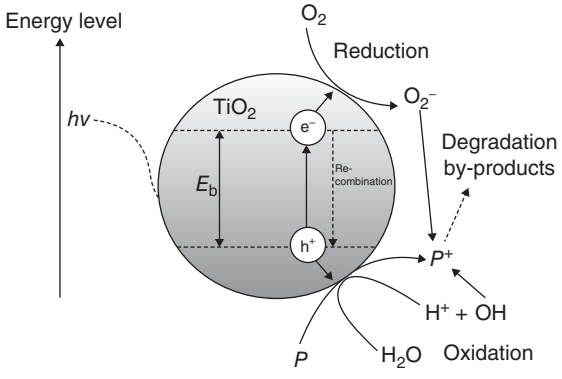

Figure 13.4 Photoinduced formation mechanism of an electron–hole pair in a semiconductor with the presence of water pollutant (P) [38]. (Chong *et al*. [38]. Reproduced with the permission of Elsevier.)

13.3.2 ILs in Photocatalysis

Numerous routes have been developed to fabricate photocatalyst nanomaterials for a photocatalysis reaction, including sol–gel, hydrothermal, anodization, solid-state chemical reaction, DC and RF magnetron sputtering, and chemical vapor deposition [13, 23, 41–43]. Many of these methods have great potential for the synthesis of photocatalyst nanomaterials in the presence of ILs. The use of ILs in chemical synthesis is an optimal way to promote and control the development of materials with controllable size and size distribution at a nanoscale and high photocatalytic activity [13, 14, 31, 40, 44, 45].

TiO_2 is the most widely used semiconductor photocatalyst to promote photoxidation reactions owing to its chemical stability in aqueous solutions, suitable band positions to induce redox reactions, and high activity under UV light. Wang *et al.* [45] synthesized TiO_2 with small crystal size in $[C_4mim][BF_4]$ IL *via* microwave radiation. The IL acted as a microwave absorption medium for preparation of TiO_2 and as extractant for dibenzothiophene (DBT), as shown in Figure 13.5 (DBT was transferred from oil to the IL phase). The proposed mechanism suggested that when $[C_4mim][BF_4]$ containing TiO_2 was irradiated by UV light, the photogenerated holes could react with water or hydroxyl groups on the surface of TiO_2 to form $^{\bullet}OH$ radicals, which photooxidized DBT to $DBTO_2$. The DBT was then transferred from oil to IL and continuously photodegraded.

One of the main challenges for heterogeneous photocatalysis is the design of visible-light-responsive photocatalysts [46]. A visible-light-induced bismuth compound photocatalyst has recently been reported [19, 21, 47]. Lv *et al.* [48] reported the synthesis of a bismuth tungstate composite (Bi_2WO_6) using a hydrothermal method and its ability to photocatalytically degrade rhodamine B in aqueous solution under visible light irradiation. Pure Bi_2WO_6 showed

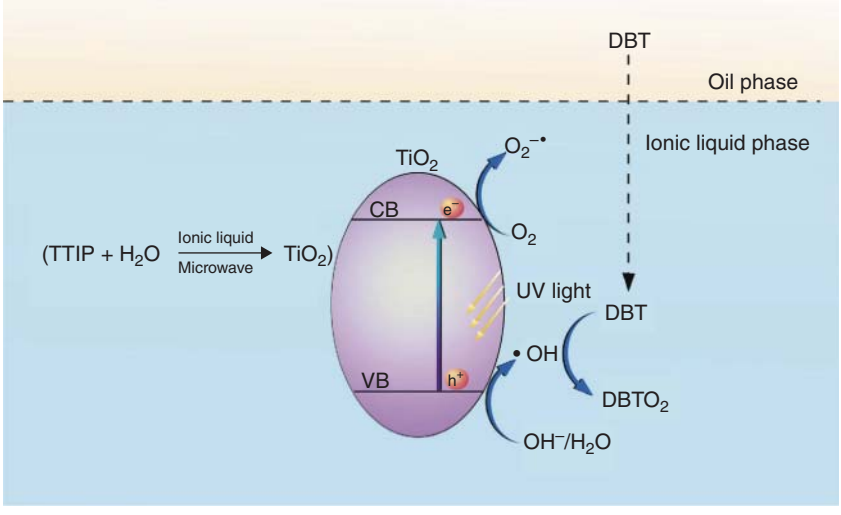

Figure 13.5 Photocatalytic oxidative desulfurization process of DBT [45]. (Wang *et al.* [45]. Reproduced with the permission of American Chemical Society.)

good activity in degrading rhodamine B. However, to improve photocatalytic activity, Bi_2WO_6 was incorporated with reduced graphene oxide (RGO) via an IL-assisted [C_4mim][BF_4] hydrothermal process. The photocatalytic activities of RGO-modified Bi_2WO_6 composites are significantly enhanced compared to pure Bi_2WO_6. In the study conducted by Lv *et al.* [48], IL acted as dispersion agent and caused Bi_2WO_6 nanoparticles to uniformly disperse on the surface of the RGO, increasing the surface area and thereby improving photocatalytic activity.

Despite the use of ILs in the synthesis of nanomaterials, recent studies have shown that they can participate effectively during the reaction to suppress the recombination of photoinduced electron-hole pairs and enhance photocatalytic response performance.

Hong *et al.* [49] fabricated α-FeOOH nanorods functionalized with 1-butyl-3-methylimidazolium chloride IL ([C_4mim][Cl]). The photocatalysts were examined for degradation of azo dye, demonstrating a 10-fold higher performance than that of commercial materials owing to the synergistic effect of well-defined nanomaterials in diffusion-controlled reactions. The key to this high performance was the fact that energy transfer in IL-functionalized nanorods facilitated a photocatalytic reaction *via* the generation of Fe^{2+}.

Zhang *et al.* [50] prepared a modified BiOI photocatalyst using the chemical precipitation method in the presence of IL. [C_4mim][I] was chosen to modify the surface of BiOI because it could act as both iodine source and surface-modifying agent. A number of studies have shown that BiOI exhibits good phocatalytic activity for the photodegradation of organic compounds under visible light irradiation. The authors evaluated the photocatalytic activities of unmodified BiOI and IL-BiOI samples by degrading methyl orange (MO) under visible light irradiation.

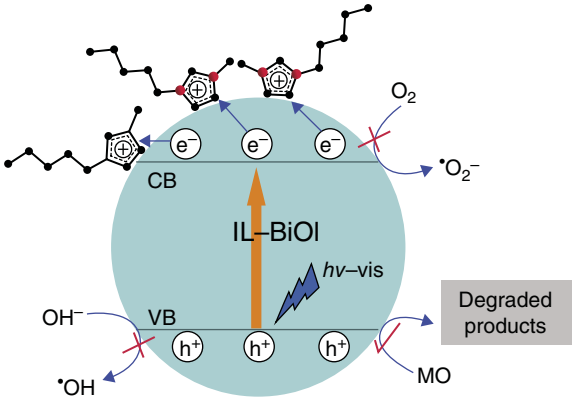

Figure 13.6 Proposed mechanism showing the catalytic role of IL on the surface of BiOI [50]. (Wang *et al.* [50]. Reproduced with permission of American Chemical Society.)

The IL-BiOI photocatalyst exhibited higher photocatalytic activity for unmodified BiOI synthesized in the absence of $[C_4mim][I]$ [50]. The enhancing effects of ILs were investigated using the photocatalysis mechanism of BiOI for photodegradation of MO. Figure 13.6 shows a schematic illustration of MO photodegradation over IL-BiOI. The authors suggested that IL modification could trap the photoexcited electron in the conduction band of BiOI to inhibit recombination of photoinduced electron–hole pairs, and thus enhance its photocatalytic activity in the degradation of organic pollutants [50].

Qi *et al.* [51] reported the synthesis of $[C_4mim][BF_4]$ on the surface of a TiO_2 sample using TiO_2 – P25 powder. They demonstrated that $[C_4mim][BF_4]/TiO_2$ is a highly efficient photocatalyst for photocatalytic degradation of MO. The IL covered the surface of TiO_2 powders, increasing the photocatalytic efficiency of TiO_2 for photodegrading MO. ILs enhance the trap and transfer of the photogenerated electrons and facilitate the adsorption of MO due to the electrostatic attraction between the positively charged $[C_4mim]^+$ ions on the surface of TiO_2 and the negatively charged MO in the solution [51].

Jin *et al.* [52] reported a heterogeneous catalyst consisting of TiO_2–P3HT–IL nanoparticles used as a photoelectrochemical (PEC)-sensing platform for the acetochlor. The catalyst was based on TiO_2 nanoparticles modified by P3HT in a room temperature IL 1-butyl-3-methylimidazolium hexafluorophosphate ($[C_4mim][PF_6]$) solution. The authors proposed a PEC method to detect acetochlor in small concentrations (ranging from 0.5 to 20 $\mu mol\, l^{-1}$). The catalyst showed excellent sensitivity in detecting acetochlor using the aforementioned PEC method. The highly sensitive detection using TiO_2–P3HT–IL rather than pure TiO_2–P3HT is due to the efficient charge separation of the TiO_2–P3HT–IL system in forming holes for the PEC oxidation of photolyzed acetochlor [52]. Figure 13.7 shows a PEC mechanism for acetochlor photoxidation under visible light irradiation. P3HT absorbs visible light to induce and transport electrons from VB to CB. The photoexcited electrons in the CB of P3HT could be injected

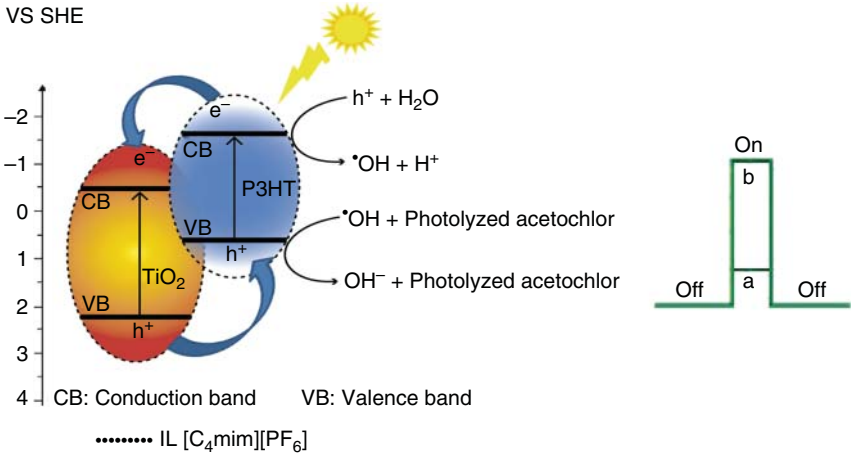

Figure 13.7 Schematic illustration of proposed photoelectrochemical mechanism for photolyzed acetochlor oxidation in TiO_2–P3HT–IL modified GCE [52]. (Jin *et al*. [52]. Reproduced with permission of Elsevier.)

into the CB of TiO_2 nanoparticles because the CB edge potentials of TiO_2 are lower than those of P3HT. The photocurrent conversion efficiency could be further amplified by the electron-transfer process from photolyzed acetochlor to P3HT through the addition of IL because of enhancement in ionic conductivity caused by the large number of free charge carriers provided by the IL [52].

Although TiO_2 has suitable band positions for photoxidation reactions, it can only utilize UV-light (~5% of the solar spectrum). To improve the absorption efficiency of TiO_2, Mirhoseini and Salabat prepared TiO_2 nanocomposites with an IL-$[C_4mim][BF_4]$-based microemulsion, which exhibited remarkable photocatalytic activity under visible light for degradation of methylene blue [53]. The authors suggested that the photo response to visible light of TiO_2 sensitized with $[C_4mim][BF_4]$ occurred because the IL molecule acts as a photon absorber in visible light and injects electrons into the conduction band of the TiO_2 photocatalyst to promote photoxidative reactions.

13.4 Water Splitting

H_2 and O_2 can be produced from water using natural energy such as sunlight, with important energy and environmental implications. As such, solar hydrogen production from water has been urged [54]. There are several ways to produce H_2 and O_2 from water and the sun: (i) electrolysis of water using a solar cell and/or hydroelectric power generation, and so on, (ii) reforming biomass, and (iii) photocatalytic or PEC WS. In all cases, the catalyst has an important role in activating the reaction. In this section of the chapter, we focus on showing the principles of

photocatalytic and PEC WS, particularly semiconductors (catalyst) synthesized in IL media.

13.4.1 Principles of Photocatalytic and Photoelectrochemical Water Splitting

The free energy necessary to split water in H_2 and O_2 gases by a WS reaction can be obtained according to Eq. (13.1).

$$H_2O \rightarrow \frac{1}{2}O_{2(g)} + H_{2(g)}; \quad \Delta G = +237 \ \text{kJ mol}^{-1} \tag{13.1}$$

According to the Nernst equation, this corresponds to $\Delta E^o = 1.23$ V per electron transferred. To use a semiconductor and drive this reaction with light, the semiconductor must absorb radiant light with photon energies of >1.23 eV (equal to wavelengths of ~1000 nm and shorter) and convert the energy into H_2 and O_2 [55]. In 1972, in the pioneering work of Honda and Fujishima [56], UV light irradiation from a TiO_2 photoelectrode in aqueous solution led to the production of H_2 and O_2 on a Pt electrode and TiO_2 photoelectrode, respectively, onto which a small electric voltage was applied. On the other hand, Bard's concept [57], which emerged in 1979, could then be applied to the design of photocatalytic systems using suspended TiO_2 particles or powders to produce H_2 and O_2 without external bias.

The electronic structure of a semiconductor plays a key role in semiconductor photoelectrocatalysis and/or photocatalysis. In both cases, when semiconductors are excited by photons with energy equal to or higher than their bandgap energy level, electrons receive energy from the photons and are thus promoted from the VB to the conduction band (CB) if the energy gain is higher than the bandgap energy level [58]. In a photocatalytic system for H_2 production, the CB level should be more negative than the H_2 production level (E_{H_2/H_2O}), while the VB should be more positive than the water oxidation level (E_{O_2/H_2O}) for efficient oxygen production from water by photocatalysis [58], as shown in Figure 13.8a. The PEC reaction is characterized by a semiconductor/electrolyte junction where an electric field is established by the energetic alignment of the Fermi level in the semiconductor and the electrochemical potential of the solution. This effect will facilitate the spatial separation of the photoexcited electron-hole pairs, Figure 13.8b. The isolated minority charge carrier migrates to surface sites at the electrolyte/semiconductor interface where redox reaction occurs. For the case depicted in Figure 13.8b,c, the photoelectrode is a photoanode where the oxygen evolution reaction (OER) occurs owing to migration of photogenerated minority carrier holes. The majority carrier electrons migrate directly to a metallic electrode (cathode), where they reduce water to H_2 (hydrogen evolution reaction, HER). The CB and VB energy values determine if a semiconductor is suitable for a nonbiased WS reaction, Figure 13.8c.

Heterogeneous photocatalytic or PEC reactions are complex systems because several simultaneous processes are needed for the reaction to proceed. The efficiency of photocatalytic and PEC WS reactions depends on three steps

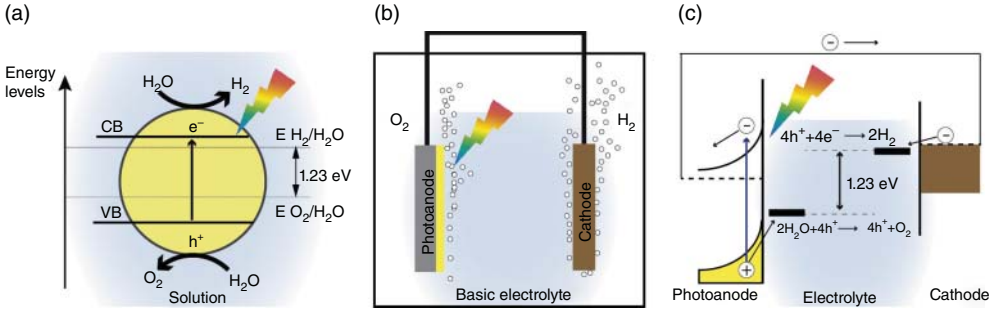

Figure 13.8 Schematic illustration of (a) photocatalytic mechanism of WS reaction for H_2 and O_2 production using an n-type semiconductor, (b) PEC WS reaction for H_2 and O_2, and (c) working principle of the PEC WS reaction with the n-type semiconductor photoanode.

between semiconductor/electrolyte interfaces that must run together to obtain maximum WS performance. The first step is photon absorption by the semiconductor to form electron–hole pairs. The second step consists of charge separation and migration of photogenerated carriers to the semiconductor surface. The third step involves surface chemical reactions, where important points include activity sites on the semiconductor surface and semiconductor surface area.

In this respect, nanostructured semiconductors usually result in a significant enhancement of photocatalytic and PEC reactions or transport rates, obtained by using small-scale dimensions (large surface area, short diffusion path, or size confinement effects). In the following subsections, we present an overview of current efforts involving photocatalytic and PEC WS reactions focusing on nanostructured semiconductors synthesized in IL media.

13.4.2
Nanostructured Semiconductor for Photocatalytic WS Reaction

Heterogeneous photocatalysts can potentially be used in H_2 production from water. However, the efficiency of this process depends on catalyst properties, nanostructure size, and geometry, and in particular the kinetics of the chemical reactions that lead to final H_2 formation. Wender *et al.* [13] reported that self-organized TiO_2 nanotube (NT) arrays are produced by Ti anodization in ethylene glycol (EG) electrolytes containing $[C_4mim][BF_4]$ IL and water. The morphology of as-formed TiO_2 NTs was considerably affected by changing anodization time, voltage, and water and IL electrolyte concentrations. The highly ordered single-walled TiO_2 NT arrays were achieved only in $EG/H_2O/[C_4mim][BF_4]$ electrolytes. This result indicates that IL has an important function in achieving high-order NTs. The TiO_2 NTs were tested as photocatalyst for H_2 evolution from a water/methanol solution by UV light irradiation, where a H_2 production rate of 0.4 μmol h^{-1} cm^{-2} was obtained. In summary, the authors conclude that

the TiO_2 NTs obtained by anodization in EG/H_2O/[C_4mim][BF_4] electrolytes have the potential to be used in hydrogen production reactions over extended periods of time.

Another important factor to obtain better H_2 production is the semiconductor crystal structure. In general, nanomaterials exhibit a single- or multiphase polycrystalline structure with very fine grain size and large grain boundaries. Concerned about these characteristics, Nagaraju *et al.* [59] described rutile phase TiO_2 nanoparticles (NPs) prepared via the ionothermal method at 120 °C using imidazolium-based functionalized IL. The authors show that the NPs obtained are a single rutile phase with crystallite size of 15 nm and nanoparticle diameter of 30 nm. The Fourier Transform Infrared Spectroscopy (FTIR) shows the presence of IL and a Ti–O–Ti peak at around 410 cm^{-1}. The UV–vis spectrum of TiO_2 nanoparticles shows blue shift compared to the bulk material. Taken together, these results indicate that TiO_2 NPs synthesized using imidazolium-based functionalized IL is a promising candidate for H_2 photocatalytic generation from water.

Rutile TiO_2-Polypyrrole (PPy) nanocomposites were prepared by *in situ* chemical polymerization of pyrrole in the presence of pure rutile phase TiO_2 NPs, where TiO_2 rutile NPs were made in water and the composite in a biphasic IL/water system [60]. PPy/TiO_2 composites in an IL/water solution increase the content ratio of TiO_2 in PPy/TiO_2 NPs, raising the ratio of H_2 produced compared with the samples produced in the toluene-water solvent system without IL media. The authors claim that the current IL-PPy/TiO_2 NP composites have potential to increase the efficiency of H_2 production through the optimization and tunability of the conducting polymer, composite morphology, and semiconductor components. The low bandgap of PPy allows the absorption of visible light and the transfer of an excited electron into the conduction band of TiO_2. The resulting electron–hole pairs split water and produce H_2 gas. These results indicate that this method can be considered a new green synthesis route to design and optimize bandgap-tunable, low-cost, efficient, and processable photocatalytic IL-PPy/TiO_2 nanomaterials for visible-light-based solar H_2 generation.

Maschmeyer *et al.* [61] describe the synthesis of crystalline CdS catalysts in different solvent systems by precipitating CdS from its ionic constituents, Cd^{2+} and S^{2-}, under ambient conditions, from an aqueous solution containing one of six tetrabutylammonium cations associate with amino acid anions (alaninate, glycinate, methioninate, serinate, threoninate, and valinate), and their subsequent photocatalytic performance for H_2 evolution. CdS nanocrystallites were shown to exhibit vastly different activities for the photocatalytic generation of H_2 in the presence of aqueous sulfurous electron donors. The most active sample was found to outperform the least active by more than 50% in terms of both turnover rate and photonic efficiency. The significant increase in performance was attributed to the differing ability of the IL solvent systems used in CdS synthesis to stabilize the reactive surfaces on the CdS crystals.

13.4.3
Nanostructured Semiconductor for the PEC WS Reaction

The best performance in PEC H_2 production is a monolithic PEC-Photovoltaic device, which exhibits 12.4% efficiency [62]. However, performance cannot be sustained because photoelectrode materials are not stable under operating conditions and undergo photocorrosion. Similar stability problems exist for most other visible-light-absorbing II–VI, III–V, and group 14 element semiconductors [36].

Today, there are strategies to develop better devices that are efficient, stable, and inexpensive. These aim at (i) coating conventional PEC cells with cocatalysts for WS or with protective layers to inhibit photocorrosion, (ii) producing the artificial leaf, a triple junction amorphous silicon cell described by Nocera [63], and (iii) developing new metal oxide materials that combine suitable properties (visible bandgap, chemical stability, high carrier mobilities, and long carrier lifetimes) for the PEC WS reaction. The third strategy can be combined with nanostructuring of the new material to improve the morphological aspects and increase the surface area.

Photoelectrodes based on nanotubular layers have been reported to be more promising than nanoparticulate layers owing to their well-defined geometry, and the feasibility to easily incorporate cocatalysts and dopants on the semiconductor surface and/or structure [64]. The surface area is a crucial factor for the enhancement of photoconversion efficiency of semiconductor nanotubular structures. Misra *et al.* [65] first demonstrated that vertically oriented double-wall TiO_2 nanotube (DW-TiO_2 NTs) arrays are synthesized by a sonoelectrochemical anodization technique in conjunction with a unique room-temperature [C_4mim][BF_4] IL and organic electrolyte, as depicted in Figure 13.9a,b. Compared to similar single-wall TiO_2 nanotubes (SW-TiO_2 NTs) (0.638 mA cm^{-2}) and commercial nanoparticles (0.365 mA cm^{-2}), these DW-TiO_2 NTs exhibit two to four times more PEC activity in splitting water under sunlight to generate H_2 and O_2, see Figure 13.9c. Another important fact is that DW-TiO_2 NTs in IL media display partial doping of B, C, and N in the TiO_2 matrix that gives rise to these NTs, which absorb visible light more efficiently than intrinsic SW-TiO_2 NTs [65, 67]. DW-TiO_2 NTs, which contain a much larger surface area than traditional SW-TiO_2 NTs, are considered to be one of the most promising nanostructures for PEC applications.

The mechanisms for the formation of DW-TiO_2 NTs and SW-TiO_2 NTs for the PEC reaction prepared at various anodizing parameters (time, voltage, temperature, etc.) in the different IL-based electrolytes were recently discussed in the literature [13, 65–72]. The mechanisms can be described for the decomposition of the anion $[BF_4]^-$to release fluoride ions into the electrolyte under the high energy field [66]. Two types of pits occur on the Ti surface during the initial anodization process as a function of the etching ability of the $[BF_4]^-$ and F^- [65]. The F^-

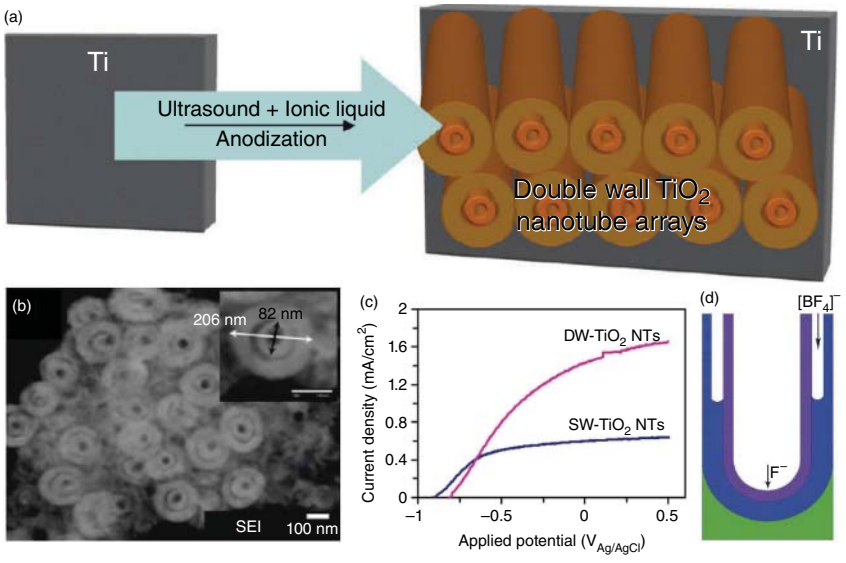

Figure 13.9 (a) Schematic illustration showing the growth of DW-TiO_2 NTs on Ti foil using the sonoelectrochemical anodization process in IL media. (b) Scanning transmission electron microscopy (STEM) surface image of DW-TiO_2 NTs. (c) Photoelectrochemical experimental data plot of annealed SW-TiO_2 NTs and DW-TiO_2 NTs under global AM1.5 in 1 M KOH electrolyte [65]. (d) Schematic diagram of DW-TiO_2 NT formation during anodization in the $[NH_4][BF_4]$-based electrolyte [66]. (John *et al*. [65]. Reproduced with permission of American Chemical Society.)

produced are more prone to react with Ti and TiO_2 at the center of the concavity than $[BF_4]^-$; thus, the bottom pore grows deeper with the fast etching rate of F^-, and the voids occur on the surrounding pore walls and continue to grow forming tubes with the slow etching rate of $[BF_4]^-$(see Figure 13.9d). The DW-TiO_2 NTs, which consist of longer inner tubes and shorter outer tubes, are then formed with the different etching rate of $[BF_4]^-$ and F^- [66].

Jing *et al.* [73] reported a simple strategy of synthesizing 1-allyl-3-(butyl-4-sulfonyl) imidazolium hydrosulfate [ABsim][HSO_4]-modified TiO_2 (IL-TiO_2) as a novel photocatalyst for PEC water OER. To confirm the concept, [ABsim][HSO_4] was used as a model IL to modify the TiO_2 bead, resulting in a covalently functionalized IL-TiO_2 composite (Figure 13.10a). In the photocurrent measured under the same conditions, the bare TiO_2 photoelectrode was much lower than that of the IL-TiO_2 photoelectrode, suggesting that IL-TiO_2 exhibits significantly higher activity toward PEC water oxidation than bare TiO_2 (Figure 13.10b). The authors attributed this effect to the presence of covalently functionalized IL cations on the TiO_2 surface while the holes generated in the VB of TiO_2 can directly transfer to the Highest Occupied Molecular Orbital (HOMO) level of the IL. On the other hand, more photoinduced electrons could be excited to the CB of TiO_2 owing to the electrostatic attraction between the positively charged cations of the IL $[ABsim]^+$ and the negatively charged electrons. As such, the

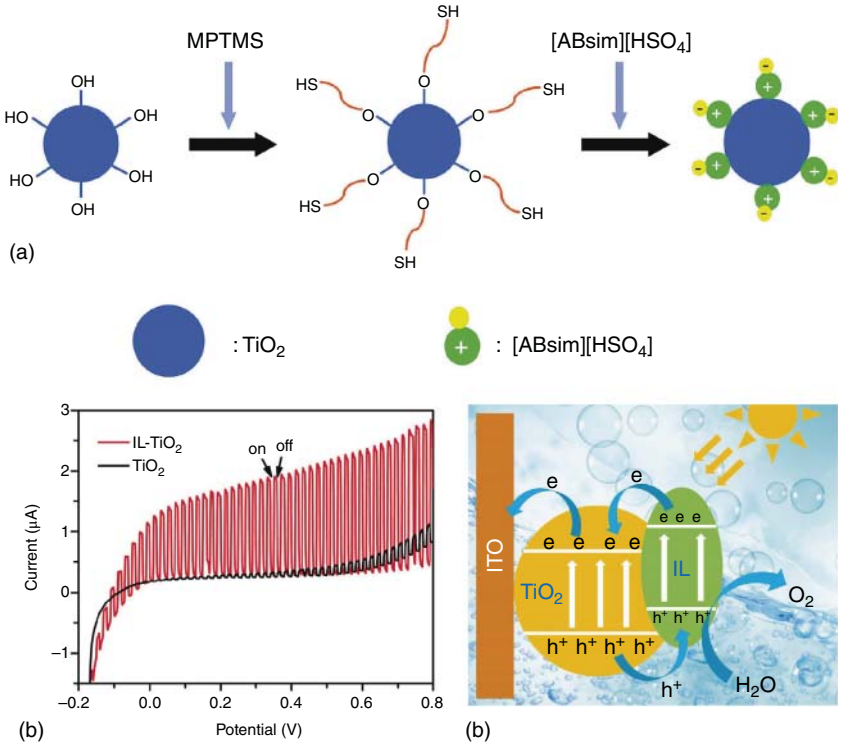

Figure 13.10 (a) Schematic illustration showing the stepwise synthetic procedure of IL-TiO_2 and (b) linear sweep voltammograms of bare TiO_2 and IL-TiO_2 under 380 nm irradiation at a scan rate of 1 mV s^{-1} under chopped light. (c) A proposed mechanism for understanding enhanced PEC water oxidation at the IL-TiO_2 photoelectrode [73]. (Jing *et al*. [73]. Reproduced with permission of Elsevier.)

electrons could be further trapped and transferred to the positively charged ITO electrode, resulting in an efficient charge separation and an easy reaction between the photoinduced holes of the IL and water to produce oxygen molecules, as can be seen in Figure 13.10c.

13.5 Summary and Conclusions

In this chapter, we highlighted three different and important processes that use the sun's energy to convert photons into electricity and decontaminate wastewater in the presence of nanocrystal semiconductors synthesized in IL media. These processes include solar cells, photocatalytic wastewater treatment, and photocatalytic and PEC WS reactions.

ILs are an important class of materials with unique and promising properties for photovoltaic applications. Because of their low volatility, high thermal and

electrochemical stability, high viscosity, and increased ionic conductivity, these special fluids have been used effectively as a primary or electrolyte additive in organic solar cells. Viscosity and ionic conductivity played important roles in high photoconversion efficiency using ILs. They have also been used to prepare solid organic solar cells, which would incur lower maintenance costs and increased physical and chemical stability. Solar cells with efficiencies above 10% show that the use of ILs in devices that convert solar energy into electricity is extremely promising and important from a scientific and technological standpoint.

Photocatalytic degradation of organic compounds is a potential route for environmental pollution control and wastewater treatment. Knowledge of the nature of photodegradation processes is crucial for the optimization of semiconductor photocatalysts, and ILs play an important role in the development of these materials. In this chapter, we have selected examples that use ILs in the synthesis of photocatalysts and as electrolytes during the photodegradation reaction. ILs play a crucial role in the preparation of materials with controllable size and size distribution at the nanoscale, thereby improving photocatalytic activity. When ILs are used as electrolytes in photodegradation reactions, they can suppress the recombination of photoinduced electron-hole pairs and enhance the photocatalytic response. Therefore, ILs can be regarded as new and tunable solvents/electrolytes with great possibilities for applications in the field of heterogeneous photocatalysis.

Photocatalytic and PEC-WS reactions demonstrated that the semiconductor catalyst has an important role in activating these reactions. The efficiency of photocatalytic and PEC-WS reactions depends on three steps: photon absorption by the semiconductor, charge separation, and migration of photogenerated carriers to the semiconductor surface and surface chemical reactions (activity sites on the semiconductor surface and surface area). It is important that these three steps run together in order to obtain maximum WS performance. In addition, the application of nanostructured semiconductors usually significantly enhances photocatalytic and PEC-WS reactions or active transport rates by using small-scale dimensions (large surface area, short diffusion path, or size confinement effects). In this respect, we demonstrated a number of examples of nanomaterials synthesized in IL media. The presence of IL induces important changes in nanocrystal structure, morphology, and surface, resulting in a functionalized composite that increases photocatalytic and/or PEC activities for H_2 generation, compared with a semiconductor synthesized in non-IL media.

References

1. Dincer, F. (2011) *Renewable Sustainable Energy Rev.*, **15**, 713–720.
2. Olah, G.A. (2005) *Angew. Chem. Int. Ed.*, **44**, 2636–2639.
3. Akorede, M.F., Hizam, H., and Pouresmaeil, E. (2010) *Renewable Sustainable Energy Rev.*, **14**, 724–734.
4. MacFarlane, D.R., Tachikawa, N., Forsyth, M., Pringle, J.M., Howlett, P.C., Elliott, G.D., Davis, J.H. Jr.,, Watanabe, M., Simon, P., and Angell, C.A. (2014) *Energy Environ. Sci.*, **7**, 232–250.
5. Dresselhaus, M.S. and Thomas, I.L. (2001) *Nature*, **414**, 332–337.

6. Beard, M.C., Luther, J.M., and Nozik, A.J. (2014) *Nat. Nanotechnol.*, **9**, 951–954.
7. Grewe, T., Meggouh, M., and Tüysüz, H. (2015) *Chem. Asian J.*, **11**, 22–42.
8. Barbir, F. (2005) *Sol. Energy*, **78**, 661–669.
9. Momirlan, M. and Veziroglu, T.N. (2005) *Int. J. Hydrogen Energy*, **30**, 795–802.
10. Elam, C.C., Padro, C.E.G., Sandrock, G., Luzzi, A., Lindblad, P., and Hagen, E.F. (2003) *Int. J. Hydrogen Energy*, **28**, 601–607.
11. Edwards, P.P., Kuznetsov, V.L., David, W.I.F., and Brandon, N.P. (2008) *Energy Policy*, **36**, 4356–4362.
12. Babatunde, E.B. (2012) *Solar Radiation, a Friendly Renewable Energy Source*, INTECH Open Access Publisher.
13. Wender, H., Feil, A.F., Diaz, L.B., Ribeiro, C.S., Machado, G.J., Migowski, P., Weibel, D.E., Dupont, J., and Teixeira, S.R. (2011) *ACS Appl. Mater. Interfaces*, **3**, 1359–1365.
14. Yoo, K., Choi, H., and Dionysiou, D.D. (2004) *Chem. Commun.*, (17), 2000–2001.
15. Hagfeldt, A., Boschloo, G., Sun, L.C., Kloo, L., and Pettersson, H. (2010) *Chem. Rev.*, **110**, 6595–6663.
16. Gratzel, M. (2003) *J. Photochem. Photobiol., C*, **4**, 145–153.
17. Kubo, W., Kitamura, T., Hanabusa, K., Wada, Y., and Yanagida, S. (2002) *Chem. Commun.*, (4), 374–375.
18. Wang, P., Zakeeruddin, S.M., Exnar, I., and Gratzel, M. (2002) *Chem. Commun.*, (24), 2972–2973.
19. Tang, J.W., Zou, Z.G., and Ye, J.H. (2004) *Catal. Lett.*, **92**, 53–56.
20. Kawano, R., Matsui, H., Matsuyama, C., Sato, A., Susan, M.A.B.H., Tanabe, N., and Watanabe, M. (2004) *J. Photochem. Photobiol., A*, **164**, 87–92.
21. Fu, H.B., Pan, C.S., Yao, W.Q., and Zhu, Y.F. (2005) *J. Phys. Chem. B*, **109**, 22432–22439.
22. Kubo, W., Makimoto, Y., Kitamura, T., Wada, Y., and Yanagida, S. (2002) *Chem. Lett.*, **31**, 948–949.
23. Akpan, U.G. and Hameed, B.H. (2010) *Appl. Catal., A*, **375**, 1–11.
24. Matsumoto, H. and Matsuda, T. (2002) *Electrochemistry*, **70**, 190–194.
25. Cao, Y., Zhang, J., Bai, Y., Li, R., Zakeeruddin, S.M., Grätzel, M., and Wang, P. (2008) *J. Phys. Chem. C*, **112**, 13775–13781.
26. Wang, P., Zakeeruddin, S.M., Comte, P., Exnar, I., and Grätzel, M. (2003) *J. Am. Chem. Soc.*, **125**, 1166–1167.
27. Wang, P., Zakeeruddin, S.M., and Grätzel, M. (2004) *J. Fluorine Chem.*, **125**, 1241–1245.
28. Usui, H., Matsui, H., Tanabe, N., and Yanagida, S. (2004) *J. Photochem. Photobiol., A*, **164**, 97–101.
29. Brennan, L.J., Barwich, S.T., Satti, A., Faure, A., and Gun'ko, Y.K. (2013) *J. Mater. Chem. A*, **1**, 8379–8384.
30. Lue, S.J., Wu, Y.-L., Tung, Y.-L., Shih, C.-M., Wang, Y.-C., and Li, J.-R. (2015) *J. Power Sources*, **274**, 1283–1291.
31. Ma, L., Chen, W.-X., Li, H., Zheng, Y.-F., and Xu, Z.-D. (2008) *Mater. Lett.*, **62**, 797–799.
32. Kim, G.-H., Kim, H.-B., Walker, B., Choi, H., Yang, C., Park, J., and Kim, J.Y. (2013) *ACS Appl. Mater. Interfaces*, **5**, 1757–1760.
33. Akpan, U.G. and Hameed, B.H. (2009) *J. Hazard. Mater.*, **170**, 520–529.
34. Chatterjee, D. and Dasgupta, S. (2005) *J. Photochem. Photobiol., C*, **6**, 186–205.
35. Fujishima, A., Rao, T.N., and Tryk, D.A. (2000) *J. Photochem. Photobiol., C*, **1**, 1–21.
36. Osterloh, F.E. (2013) *Chem. Soc. Rev.*, **42**, 2294–2320.
37. Chen, X.B., Shen, S.H., Guo, L.J., and Mao, S.S. (2010) *Chem. Rev.*, **110**, 6503–6570.
38. Chong, M.N., Jin, B., Chow, C.W.K., and Saint, C. (2010) *Water Res.*, **44**, 2997–3027.
39. Rossi, L.M., Costa, N.J.S., Silva, F.P., and Gonçalves, R.V. (2013) *Nanotechnol. Rev.*, **2**, 597.
40. Wang, W., Shen, J., Li, N., and Ye, M. (2013) *Mater. Lett.*, **106**, 284–286.
41. Chhabra, V., Pillai, V., Mishra, B.K., Morrone, A., and Shah, D.O. (1995) *Langmuir*, **11**, 3307–3311.
42. Nian, J.-N. and Teng, H. (2006) *J. Phys. Chem. B*, **110**, 4193–4198.
43. Meng, L.-J. and dos Santos, M.P. (1993) *Thin Solid Films*, **226**, 22–29.

44. Nagaraju, G., Ebeling, G., Gonçalves, R.V., Teixeira, S.R., Weibel, D.E., and Dupont, J. (2013) *J. Mol. Catal. A: Chem.*, **378**, 213–220.
45. Wang, X.-j., Li, F.-t., Liu, J.-x., Kou, C.-g., Zhao, Y., Hao, Y.-j., and Zhao, D. (2012) *Energy Fuels*, **26**, 6777–6782.
46. Martha, S., Chandra Sahoo, P., and Parida, K.M. (2015) *RSC Adv.*, **5**, 61535–61553.
47. Zhou, L., Wang, W.Z., Liu, S.W., Zhang, L.S., Xu, H.L., and Zhu, W. (2006) *J. Mol. Catal. A: Chem.*, **252**, 120–124.
48. Lv, H., Liu, Y., Hu, J., Li, Z., and Lu, Y. (2014) *RSC Adv.*, **4**, 63238–63245.
49. Park, H., Lee, Y.-C., Choi, B.G., Choi, Y.S., Yang, J.-W., and Hong, W.H. (2010) *Small*, **6**, 290–295.
50. Wang, Y., Deng, K., and Zhang, L. (2011) *J. Phys. Chem. C*, **115**, 14300–14308.
51. Qi, L., Yu, J., and Jaroniec, M. (2013) *Adsorption*, **19**, 557–561.
52. Jin, D., Xu, Q., Wang, Y., and Hu, X. (2014) *Talanta*, **127**, 169–174.
53. Mirhoseini, F. and Salabat, A. (2015) *RSC Adv.*, **5**, 12536–12545.
54. Kudo, A. and Miseki, Y. (2009) *Chem. Soc. Rev.*, **38**, 253–278.
55. Walter, M.G., Warren, E.L., McKone, J.R., Boettcher, S.W., Mi, Q.X., Santori, E.A., and Lewis, N.S. (2010) *Chem. Rev.*, **110**, 6446–6473.
56. Fujishima, A. and Honda, K. (1972) *Nature*, **238**, 37–38.
57. Bard, A.J. (1979) *J. Photochem.*, **10**, 59–75.
58. Ni, M., Leung, M.K.H., Leung, D.Y.C., and Sumathy, K. (2007) *Renewable Sustainable Energy Rev.*, **11**, 401–425.
59. Nagaraju, G., Ravishankar, T.N., Manjunatha, K., Sarkar, S., Nagabhushana, H., Goncalves, R., and Dupont, J. (2013) *Mater. Lett.*, **109**, 27–30.
60. Tan, Y., Chen, Y., Mahimwalla, Z., Johnson, M.B., Sharma, T., Bruening, R., and Ghandi, K. (2014) *Synth. Met.*, **189**, 77–85.
61. Lau, V.W.-h., van de Water, L.G.A., Masters, A.F., and Maschmeyer, T. (2012) *Chem. Eur. J.*, **18**, 2923–2930.
62. Khaselev, O. and Turner, J.A. (1998) *Science*, **280**, 425–427.
63. Nocera, D.G. (2012) *Acc. Chem. Res.*, **45**, 767–776.
64. Lee, K., Mazare, A., and Schmuki, P. (2014) *Chem. Rev.*, **114**, 9385–9454.
65. John, S.E., Mohapatra, S.K., and Misra, M. (2009) *Langmuir*, **25**, 8240–8247.
66. Li, H., Xing, J., Xia, Z., and Chen, J. (2014) *RSC Adv.*, **4**, 23214–23217.
67. Liu, Y., Mu, K.S., Yang, G., Peng, H., Shen, F., Wang, L.L., Deng, S.H., Zhang, X.H., and Zhang, Y.Z. (2015) *New J. Chem.*, **39**, 3923–3928.
68. Xing, J.H., Li, H., Xia, Z.B., Chen, J.Q., Zhang, Y.H., and Zhong, L. (2014) *Ind. Eng. Chem. Res.*, **53**, 10667–10672.
69. Xing, J.H., Li, H., Xia, Z.B., Chen, J.Q., Zhang, Y.H., and Zhong, L. (2014) *Electrochim. Acta*, **134**, 242–248.
70. Li, H., Xing, J., Xia, Z., and Chen, J. (2014) *Electrochim. Acta*, **139**, 331–336.
71. Freitas, R.G., Santanna, M.A., and Pereira, E.C. (2014) *J. Power Sources*, **251**, 178–186.
72. Freitas, R.G., Santanna, M.A., and Pereira, E.C. (2014) *Electrochim. Acta*, **136**, 404–411.
73. Jing, L., Wang, M., Li, X., Xiao, R., Zhao, Y., Zhang, Y., Yan, Y.-M., Wu, Q., and Sun, K. (2015) *Appl. Catal., B*, **166**, 270–276.